Frontiers of Information Technology & Electronic Engineering
www.jzus.zju.edu.cn; engineering.cae.cn; www.springerlink.com
ISSN 2095-9184 (print); ISSN 2095-9230 (online)
E-mail: jzus@zju.edu.cn

Optical plasma boundary reconstruction based on least squares for EAST Tokamak*

Hao LUO[1], Zheng-ping LUO[2], Chao XU[1], Wei JIANG‡[1]

[1]*Institute of Cyber-Systems and Control, Zhejiang University, Hangzhou 310027, China*

[2]*Institute of Plasma Physics, Chinese Academy of Sciences, Hefei 230031, China*

E-mail: haoluocsc@zju.edu.cn; zhpluo@ipp.ac.cn; cxu@zju.edu.cn; jiangwei@iipc.zju.edu.cn

Received Jan. 14, 2017; Revision accepted Mar. 14, 2017; Crosschecked July 8, 2018; Published online Sept. 12, 2018

Abstract: Reconstructing the shape and position of plasma is an important issue in Tokamaks. Equilibrium and fitting (EFIT) code is generally used for plasma boundary reconstruction in some Tokamaks. However, this magnetic method still has some inevitable disadvantages. In this paper, we present an optical plasma boundary reconstruction algorithm. This method uses EFIT reconstruction results as the standard to create the optimally optical reconstruction. Traditional edge detection methods cannot extract a clear plasma boundary for reconstruction. Based on global contrast, we propose an edge detection algorithm to extract the plasma boundary in the image plane. Illumination in this method is robust. The extracted boundary and the boundary reconstructed by EFIT are fitted by same-order polynomials and the transformation matrix exists. To acquire this matrix without camera calibration, the extracted plasma boundary is transformed from the image plane to the Tokamak poloidal plane by a mathematical model, which is optimally resolved by using least squares to minimize the error between the optically reconstructed result and the EFIT result. Once the transform matrix is acquired, we can optically reconstruct the plasma boundary with only an arbitrary image captured. The error between the method and EFIT is presented and the experimental results of different polynomial orders are discussed.

Key words: Optical boundary reconstruction; Boundary detection; Global contrast; Least square; EAST Tokamak
https://doi.org/10.1631/FITEE.1700041 **CLC number:** TP317.4

1 Introduction

Economically affordable, environmentally sustainable, and politically acceptable (Pironti and Walker, 2005) nuclear fusion is expected to become a promising source of energy to support the increasing world demand in the future. The Tokamak is a device using magnetic confinement to achieve controlled nuclear fusion. There are a lot of unresolved problems in the research of plasma discharge in the Tokamak. Optical diagnostic techniques have increasingly been applied to control plasma discharge. Recently, most of Tokamaks, such as TCV (Hommen et al., 2010, 2013, 2014), ITER (Kumar et al., 2012; Perek, 2013), NSTX (Davis et al., 2010), EAST (Xue et al., 2011; Zhu et al., 2016), and other Tokamaks (Zweben et al., 2011; Hussain et al., 2016), have been equipped with image acquisition systems. There are three main kinds of optical diagnostic techniques in Tokamaks.

The first one uses infrared (IR) cameras to monitor and measure the high heat fluxes or heat deposits (Mitteau et al., 2007; Qi et al., 2008; Ahn et al., 2010; Martin et al., 2010). In Tokamaks, the plasma-facing components (PFCs), the first wall directly facing the Tokamak plasma, are subjected to high heat fluxes that can damage them. In current Tokamaks, IR thermographic diagnostics based on image analysis

‡ Corresponding author

* Project supported by the National Natural Science Foundation of China (Nos. 61375049 and 61473253)

ORCID: Hao LUO, http://orcid.org/0000-0002-6405-4011

and feedback control are used to measure and monitor the heating of the PFCs during plasma operation. IR cameras are set on the Tokamak to capture IR images. In IR images, the IR luminance is relative to the temperature. With the feature of luminance, the temperature map of PFCs can be evaluated and then compared with the heat flux model. The heat fluxes and heat deposits can also be measured.

The second main application of optical diagnostics in Tokamaks is to use high-speed cameras to measure the velocity field of articles in the Tokamak, which is called the particle tracking velocimetry (PTV) (Munsat and Zweben, 2006; Odstrcil et al., 2013; Alpers et al., 2015). In the Tokamak discharge experiments, it is difficult to obtain the fluid dynamics of plasma directly. Particle tracking and dust tracking are playing important roles in studying plasma in Tokamaks. Light is scattered from the tracer particles in this laser sheet and imaged on a charge coupled device (CCD) camera. From two consecutive images, we can obtain 2D flow velocities in the plane of the laser sheet. Then the 2D velocities can be developed into 3D velocities in different ways with different 3D PTV modes.

The third main application is using high-speed CCD cameras to optically reconstruct the plasma boundary (Xue et al., 2011; Hommen et al., 2013, 2014). Control of plasma position and shape play important roles in plasma discharge in Tokamaks. In nuclear fusion plasma, the plasma position and shape are often estimated by using equilibrium and fitting (EFIT) code and provided to a real-time control system for position and shape control. However, there will be a significant error with extended plasma discharge due to the integral drift of this measurement. High-speed CCD cameras are set on Tokamaks to capture real-time plasma images. Using image processing methods, the plasma boundary is extracted from images. Then the extracted boundary should be reconstructed in the Tokamak poloidal plane for the feedback control system.

The research of this paper is the third application of optical plasma boundary reconstruction for the experimental advanced superconducting Tokamak (EAST). EAST is an advanced steady-state plasma physics experimental device that was built at the Institute of Plasma Physics, Chinese Academy of Sciences (ASIPP). The TCV Tokamak has used a similar optical technique proposed by G. Hommen in the past few years. Hommen et al. (2013) named this optical technique OFIT and improved it as RT-OFIT (Hommen et al., 2014), which is applied to a real-time control system.

However, OFIT uses only a simple gradient operator to extract the edge. If the images do not have high resolution and contrast, there will be some false edges in the results. In addition, camera calibration is necessary for OFIT to transform the plasma boundary extracted from the image plane to the Tokamak poloidal plane. The parameters of the camera model are calibrated manually by minimizing the distance between the observed and predicted pixel coordinates of a number of Tokamak structures that are identified in the image. This is a complex problem and the error of optical reconstruction depends on the accuracy of camera calibration.

In this study, we present a new optical plasma boundary reconstruction method that does not require camera calibration. First, we preprocess the image and set some regions of interest (ROIs) manually. In the image, plasma boundaries of each ROI are extracted by the edge detection algorithm based on global contrast proposed here. Those boundaries can build up a full boundary. We propose a mathematical optimization model based on least squares to transform the boundary to the Tokamak poloidal plane without camera calibration. The goal is to minimize the distance between the optical reconstruction and the EFIT results. All our work is based on discharge experiments and EFIT data of the EAST Tokamak.

2 Video capture system of the EAST Tokamak

EAST is the first fully superconducting Tokamak designed by China with modern diverter configurations in the world. The design parameters of EAST include a major radius of 1.7 m, a minor radius of 0.4 m, a plasma current of 1 MA, a toroidal field of 3.5 T, and a pulse length of 1000 s.

With the development of Tokamak optical diagnostic techniques, EAST designs a video capture system to reconstruct the plasma boundary optically. Two high-speed CCD cameras are set on the horizontal port of the Tokamak. These cameras are the AT-200CL and Falcon 1M120 HG industrial camera, respectively. The Falcon 1M120 HG camera has a

high frame rate. Its sampling frame rate can reach more than 100 frames/s. The AT-200CL camera has high resolution, with two megapixels of three CCD channels. A complete discharge video of 10 s duration and 680 × 544 pixels can be acquired and saved by the EAST video capture system. Fig. 1 shows the video images and each image represents a period of 1 s in the sequence. The initial two seconds are in the rising period of the discharge experiment; the plasma boundary is irregular, unstable, and unclear. The last two seconds are in the falling period of the discharge experiment; the plasma gradually breaks up and illumination becomes lower and lower. Neither of these periods is suitable for optical plasma boundary reconstruction. In addition, the outer plasma boundary is incomplete and unclear. Only the inner plasma boundary is reconstructed in this study.

3 Plasma boundary detection

To optically reconstruct the plasma boundary, the boundary must be extracted from the captured video using an image processing method. Before plasma boundary detection, the image should be preprocessed for a better result. Taking into account that the plasma boundary is a kind of slowly changing edge, we propose an edge detection algorithm based on global contrast. Compared with the TCV plasma boundary detection method, this algorithm can extract the plasma boundary better in most cases, especially when the image contrast or illumination is poor.

3.1 Image preprocessing

In addition to the plasma boundary, some other boundaries are presented in the image, such as the reactor wall. This useless information will interfere with the plasma boundary detection. Hommen et al. (2013) proposed the ROI to solve this problem. Each ROI covers a region of the image, where a single segment of the plasma boundary is expected. These ROIs are set manually and meet the following requirements: (1) camera position, focus, vision, and other parameters are fixed and the ROIs of each frame are unchanged; (2) each ROI covers parts of the unique and clear plasma boundary; (3) each ROI is as small as possible but can cover the plasma boundary of each frame as much as possible. The shape of the ROI is rectangular for convenience. According to these requirements, Fig. 2a shows all the ROIs. There are two main effects. One is to improve the accuracy of edge detection. As mentioned earlier, there are some other boundaries in the image. Artificially excluding these boundaries as invalid information can greatly improve detection accuracy. The other one is to speed up the computing process. Because only a part of the area must be processed, the amount of calculation is reduced, which improves the speed of edge extraction. Apart from setting the ROI manually, another preprocessing technique is color image gray processing. The original images captured by the EAST Tokamak video capture system are three-channel color digital images. The practical edge detection process does not need the complete three-channel information. A common practice is to transform color images into gray-scale images that integrate three channels of information. It reduces the calculation by two-thirds. Fig. 2b shows the gray-scale image.

3.2 Edge extraction based on global contrast

Because the plasma boundary changes slowly, the traditional edge detection algorithms based on the gradient operator cannot obtain good results to reconstruct plasma boundary optically. The extracted information includes many false edges. However, plasma edge pixels generally have a high luminance value, which means a high global contrast. Thus, we propose an edge detection algorithm based on global contrast to extract the plasma boundary. Specifically, the significant value of a pixel is defined by its contrast with the other pixels. Fig. 3 shows

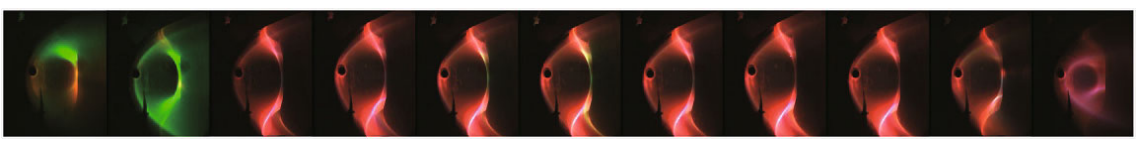

Fig. 1 Video images. The images represent 0–10 s shots in order. References to color refer to the online version of this figure

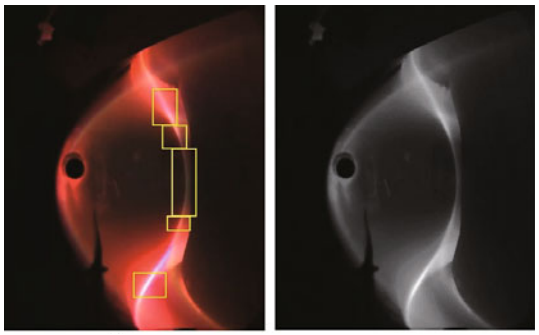

Fig. 2 ROI of the plasma boundary (yellow box) (a) and gray-scale image of the EAST Tokamak plasma (b). References to color refer to the online version of this figure

the plasma boundary detection process of one ROI. Fig. 3a shows the gray-scale image of the ROI.

For an image $\boldsymbol{I}$ with $m \times n$ pixels, the significant value $s(x, y)$ of pixel $I(x, y)$ is

$$s(x,y) = \ln(I(x,y)+1) \sum_{i=1}^{m} \sum_{j=1}^{n} (I(x,y) - I(i,j)), \quad (1)$$

where $I(x, y)$ denotes the gray-scale value of the pixel in row x and column y, and $I(i, j)$ has the same meaning.

However, calculating the $s(x, y)$ of one pixel requires scanning the entire image, and calculating the significant values of all pixels requires scanning the entire image twice, which is a time-consuming process. To improve the computational efficiency, Eq. (1) can be rearranged as follows:

$$\begin{aligned} s(x,y) &= \ln(I(x,y)+1) \sum_{i=1}^{m} \sum_{j=1}^{n} (I(x,y) - I(i,j)) \\ &= \ln(I(x,y)+1) \left(mnI(x,y) - \sum_{i=1}^{m} \sum_{j=1}^{n} I(i,j) \right) \\ &= mn \ln(I(x,y)+1)(I(x,y) - \overline{I}), \end{aligned} \quad (2)$$

where $\overline{I}$ is the average gray-scale value of image $\boldsymbol{I}$. The $\overline{I}$ value is a count for an image, which means that computing $s(x, y)$ requires several simple mathematical operations rather than scanning the entire image. Therefore, computational efficiency is greatly improved. We can calculate a corresponding edge significant map for each ROI. For the same ROI, the significant degree of each boundary pixel is positively related to its significant value. However, it is difficult to use the same scale to compare different ROIs.

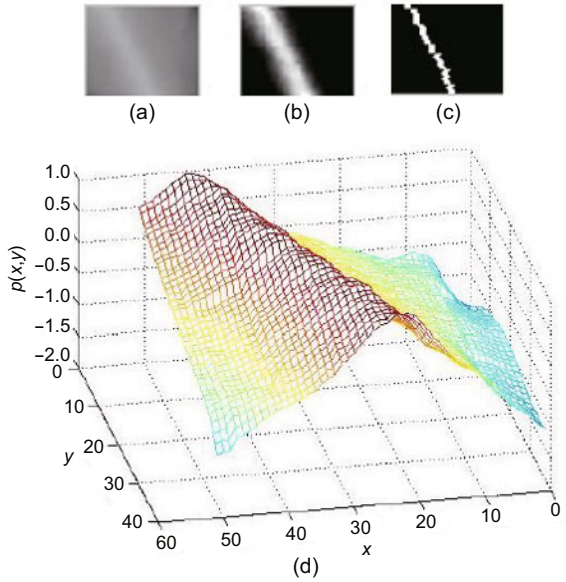

Fig. 3 Plasma boundary detection process of one ROI: (a) original gray-scale image; (b) probability graph; (c) plasma boundary detection result; (d) secondary surface $\boldsymbol{p(x, y)}$

Thus, the edge significant map is transformed to an edge probability graph, which is defined as

$$p(x,y) = \frac{s(x,y)}{s_{\max}(x,y)}, \quad (3)$$

where $p(x, y)$ is the edge probability function, which represents the probability of a plasma boundary for each pixel. However, this is just a generalized probability value; the maximum value is 1, and the minimum is not 0 but rather an unknown negative. The value of the actual probability distribution ranges from 0 to 1. The part of $p(x, y)$ which is less than 0 is taken as 0 when the probability graph is shown intuitively in Fig. 3b. In the probability graph, the edge feature of the plasma boundary is significantly enhanced by calculating global contrast. As shown in Fig. 3d, the edge probability function $p(x, y)$ in a three-dimensional coordinate system is a typical mountain-type surface longitudinally, where the plasma boundary is the mountain ridge. The longitudinal mountain ridge of a mountain ridge-type secondary surface can be approximated mathematically as a set of points $\mathrm{d}p/\mathrm{d}x = 0$. Taking into account that $p(x, y)$ is a discrete two-dimensional matrix, the plasma boundary pixels can be considered equivalently as a set of points that are the maximum of each row of the edge probability matrix. Fig. 3c shows the final edge detection of such an ROI result.

The plasma boundaries of the remaining ROIs can be extracted similarly and are shown in Fig. 4, where some large ROIs are divided into several small ROIs for convenience.

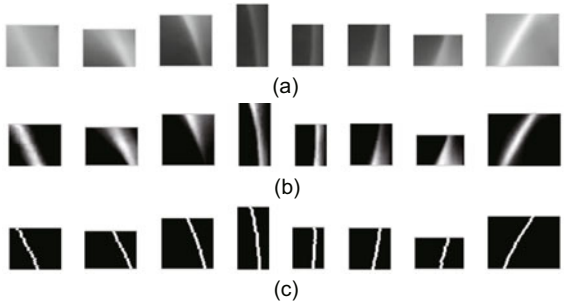

Fig. 4 Plasma boundary detection of all ROIs: (a) original gray-scale images; (b) probabilities graphs; (c) edge detection results

After extracting the plasma boundary of each ROI, the complete results can be acquired by splicing all parts of edges. Fig. 5 shows the complete results. Fig. 5a is a low-intensity image, whereas Fig. 5b is a high-intensity image. In Fig. 5, illumination in the edge detection algorithm based on global contrast is robust because the image contrast is stretched by the global contrast.

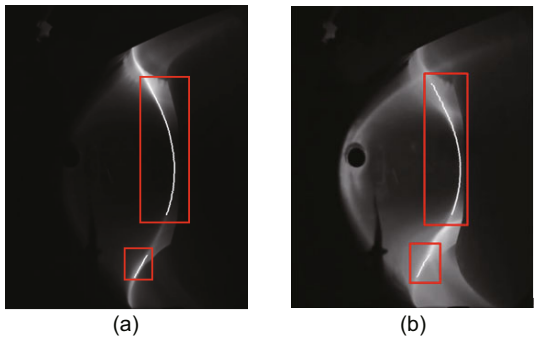

Fig. 5 Plasma boundary detection results of all ROIs: (a) low-intensity image; (b) high-intensity image

To further verify the effectiveness of the algorithm proposed in this study, Fig. 6 shows a comparison of traditional edge detection algorithms and our algorithm. As can be seen, traditional first-order algorithms, such as Roberts, Prewitt, and Sobel, cannot extract the plasma boundary. There are not only some unclear plasma boundaries but also many false edges. The second-order Canny algorithm (Canny, 1986) performs a little better than first-order algorithms. Although the plasma boundary extracted is comparatively clear, there are some false edges

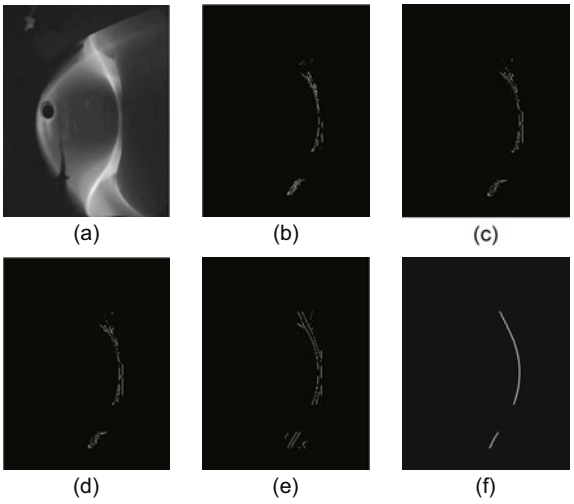

Fig. 6 Various edge extraction algorithm results: (a) gray-scale image; (b) Roberts algorithm; (c) Prewitt algorithm; (d) Sobel algorithm; (e) Canny algorithm; (f) our algorithm

presented in the resulting image. Obviously, our proposed algorithm based on global contrast can acquire a single and clear plasma boundary.

3.3 Comparison of EAST and TCV plasma boundary detection

The TCV Tokamak first reconstructed the optical plasma boundary and announced the edge detection algorithm applied in actual real-time feedback control. TCV used a vertical gradient edge detection operator with filtering capabilities (Hommen et al., 2013). The operator and filtering capabilities are

$$\mathrm{Op}=\begin{bmatrix}1 & 2 & 3 & 0 & -3 & -2 & -1\\ 1 & 2 & 3 & 0 & -3 & -2 & -1\\ 1 & 2 & 3 & 0 & -3 & -2 & -1\end{bmatrix}, \tag{4}$$

$$\boldsymbol{I}_{\mathrm{after}}=\boldsymbol{I}_{\mathrm{before}}\otimes\mathrm{Op}, \tag{5}$$

where $\boldsymbol{I}_{\mathrm{after}}$ denotes the image after processing, $\boldsymbol{I}_{\mathrm{before}}$ denotes the image before processing, and $\otimes$ denotes the matrix convolution operation.

Using this operator to convolute the image can produce a gradient image in which plasma boundary pixels have high gradient values. Then the edge feature can be extracted by determining the segmentation threshold. The TCV operator is used to convolute with the captured EAST image to extract the plasma boundary with a high threshold (HT) and a low threshold (LT), respectively. Fig. 7 shows the results.

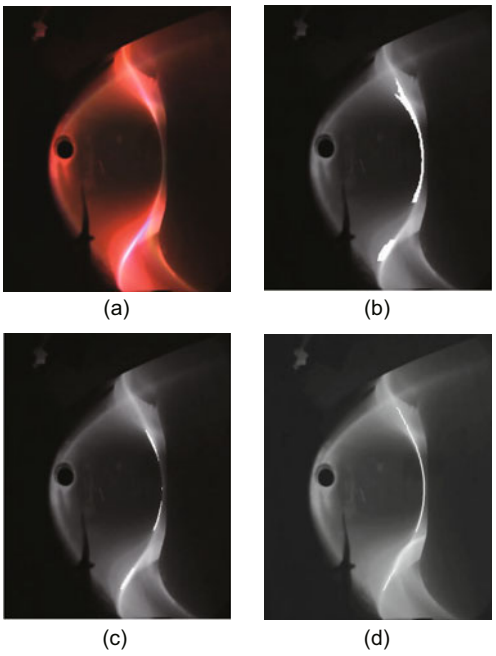

Fig. 7 Comparison of the EAST plasma boundary: (a) EAST image; (b) TCV algorithm with a low threshold; (c) TCV algorithm with a high threshold; (d) our algorithm

The white pixels are the edges extracted. Although the TCV algorithm can position the plasma boundary well to a degree, there are many false edges when the segmentation threshold is low, and many true edges are lost when the threshold is too high. Clearly, our algorithm (Fig. 7d) has a better result. When images have high quality, such as high contrast or suitable intensity, the TCV convolution operator will detect the plasma boundary well. Furthermore, using our method and the TCV method respectively, the TCV image is handled without high contrast. Fig. 8 shows the comparison. Similarly, our algorithm (Fig. 8d) has a better effect. In summary, edge detection based on global contrast can solve the issue of plasma boundary detection well.

4 Plasma boundary reconstruction

In Section 3, we describe how to extract the plasma boundary from the captured Tokamak discharge images, but the extracted boundary is in the image plane. The actual real-time feedback plasma control system requires the plasma boundary position should be in the Tokamak poloidal plane. In this section, we describe how to transform the extracted boundary from the image plane to the poloidal plane.

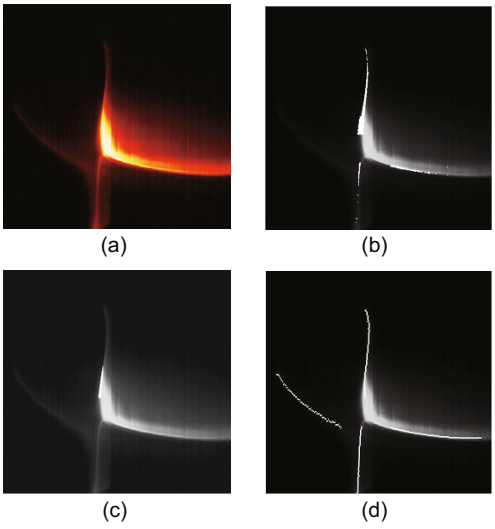

Fig. 8 Comparison of the TCV plasma boundary: (a) TCV image; (b) TCV algorithm with a low threshold; (c) TCV algorithm with a high threshold; (d) our algorithm

Usually, it can be solved simply by camera calibration. The camera calibration method (Zhang, 2000) just needs to take a few photos of the calibration plate.

However, it is difficult to set a calibration plate in the Tokamak device for calibration. Although we can select a number of feature points in the wall of the reactor as the calibration points to approximate calibration parameters, it is still a complex optimization problem. In this study, we propose a plasma boundary reconstruction model that does not require camera calibration and that is based on least squares to transform the extracted boundary from the image plane to the Tokamak poloidal plane.

4.1 Plasma boundary reconstruction of one single frame

If we obtain a binary image containing only the plasma boundary, we can obtain the coordinates of edge pixels in the image coordinate system. The abscissa and ordinate of the pixels are respectively equal to the number of rows and columns. The rows and columns of all edge pixels can be represented respectively by vector $\boldsymbol{x} = [x_1, x_2, \ldots, x_i]^{\mathrm{T}}$ and vector $\boldsymbol{y} = [y_1, y_2, \ldots, y_i]^{\mathrm{T}}$, where i is the number of edge pixels. The plasma boundary in the image plane is represented mathematically and approximately by an l^{th}-order polynomial:

$$y_i = a_l x_i^{l-1} + a_{l-1} x_i^{l-2} + \cdots + a_1, \qquad (6)$$

where $\boldsymbol{a} = [a_l, a_{l-1}, \ldots, a_1]$ is the coefficient vector of the polynomial. The abscissa of the plasma boundary reconstructed by EFIT in the r-z poloidal plane is $\boldsymbol{z} = [z_1, z_2, \ldots, z_j]$ and the ordinate is $\boldsymbol{r} = [r_1, r_2, \ldots, r_j]$, where j is the amount of edge data reconstructed by EFIT. The boundary reconstructed by EFIT can be represented by an l^{th}-order polynomial and the coefficient vector is $\boldsymbol{b} = [b_l, b_{l-1}, \ldots, b_1]$. Then the problem is finding the transition matrix $\boldsymbol{W}$ to predict the approximate coefficient vector $\widetilde{\boldsymbol{b}}$:

$$\widetilde{\boldsymbol{b}} = [\widetilde{b}_l, \widetilde{b}_{l-1}, \ldots, \widetilde{b}_1] = \boldsymbol{a}\boldsymbol{W}, \tag{7}$$

and the reconstructed poloidal plane coordinates are

$$\begin{cases} \widetilde{r}_1 = \widetilde{b}_l z_1^{l-1} + \widetilde{b}_{l-1} z_1^{l-2} + \cdots + \widetilde{b}_1, \\ \widetilde{r}_2 = \widetilde{b}_l z_2^{l-1} + \widetilde{b}_{l-1} z_2^{l-2} + \cdots + \widetilde{b}_1, \\ \quad \vdots \qquad\quad \vdots \\ \widetilde{r}_j = \widetilde{b}_l z_j^{l-1} + \widetilde{b}_{l-1} z_j^{l-2} + \cdots + \widetilde{b}_1. \end{cases} \tag{8}$$

To find $\boldsymbol{W}$, the loss function is built as

$$\begin{aligned} L &= \sum_{k=1}^{j} \|\widetilde{r}_k - r_k\|_2^2 \\ &= \sum_{k=1}^{j} \|\boldsymbol{a}\boldsymbol{W}[z_k^l, z_k^{l-1}, \ldots, z_k^1]^{\mathrm{T}} - r_k\|_2^2 \\ &= \sum_{k=1}^{j} \|\boldsymbol{a}\boldsymbol{W}\boldsymbol{z}_k - r_k\|_2^2. \end{aligned} \tag{9}$$

To make the reconstruction result as close to the EFIT result as possible, $\boldsymbol{W}$ should satisfy

$$\boldsymbol{W} = \arg\min_{\boldsymbol{W}} L. \tag{10}$$

This is a typical least squares problem and $\boldsymbol{W} \in \mathbb{R}^{(l+1)\times(l+1)}$ is a matrix with $(l+1)^2$ unknown parameters. Usually, the polynomial order is not very high, so $(l+1)^2$ is less than j. The function does not have a unique solution, but we can find an approximate least squares solution. Suppose

$$\begin{aligned} \boldsymbol{Z}_l &= [\boldsymbol{z}_1, \boldsymbol{z}_2, \ldots, \boldsymbol{z}_j] \\ &= \begin{bmatrix} z_1^l & z_2^l & \cdots & z_j^l \\ z_1^{l-1} & z_2^{l-1} & \cdots & z_j^{l-1} \\ \vdots & \vdots & & \vdots \\ z_1^1 & z_2^1 & \cdots & z_j^1 \end{bmatrix}. \end{aligned} \tag{11}$$

Then the system of linear equations can be simply expressed as

$$\boldsymbol{a}\boldsymbol{W}\boldsymbol{Z}_l = \boldsymbol{r}, \tag{12}$$

where $\boldsymbol{W}$ is the optimal solution for optical reconstruction. $\boldsymbol{W}$ can be solved by singular value decomposition (SVD):

$$\boldsymbol{W} = \boldsymbol{a}^{+}\boldsymbol{r}\boldsymbol{Z}_l^{+} = \boldsymbol{V}_{\boldsymbol{a}}\boldsymbol{\Sigma}_{\boldsymbol{a}}^{+}\boldsymbol{U}_{\boldsymbol{a}}^{*}\boldsymbol{r}\boldsymbol{V}_{\boldsymbol{Z}_l}\boldsymbol{\Sigma}_{\boldsymbol{Z}_l}^{+}\boldsymbol{U}_{\boldsymbol{Z}_l}^{*}, \tag{13}$$

where $\boldsymbol{V}_{\boldsymbol{a}}$, $\boldsymbol{\Sigma}_{\boldsymbol{a}}^{+}$, $\boldsymbol{U}_{\boldsymbol{a}}^{*}$ and $\boldsymbol{V}_{\boldsymbol{Z}_l}$, $\boldsymbol{\Sigma}_{\boldsymbol{Z}_l}^{+}$, $\boldsymbol{U}_{\boldsymbol{Z}_l}^{*}$ are the SVD matrices of $\boldsymbol{a}$ and $\boldsymbol{Z}_l$, respectively. If we know the coefficient vector $\boldsymbol{a}$ of the polynomial of the plasma boundary in the image plane and the r-z coordinates reconstructed by EFIT in the poloidal plane, the optimal transition matrix $\boldsymbol{W}$ can be easily solved. Then optical reconstruction results can be acquired. The reconstruction error is

$$\text{error} = \frac{1}{j}\sum_{k=1}^{j} |\boldsymbol{a}\boldsymbol{W}\boldsymbol{z}_k - r_k|. \tag{14}$$

We have reconstructed 704 frames of image data from the test sample database with different orders. The database will be introduced in detail in the next subsection. Table 1 shows the results.

Table 1 Errors of different orders for single frame reconstruction

Order	Error (m)		
	Maximum	Average	Minimum
2	0.0160	0.0135	0.0098
3	0.0109	0.0087	0.0063
4	0.0085	0.0070	0.0050
5	0.0085	0.0070	0.0050

When the order is not more than four, the reconstruction error is reduced with the increasing order. It is interesting that the results of the fourth order and fifth order are the same. This means that the highest reconstruction order is four and higher orders will not obtain better results. The following is an example of single frame reconstruction. When the polynomial order is four, the optical reconstruction results of the 5.74 s image of the 52 039-shot discharge video are shown in Fig. 9.

For a single image, our proposed reconstruction model has good effect and obtains results that are similar to those of EFIT. In all 44 sample points, only seven point errors are larger than 1 cm, and the remaining 37 are not larger than 1 cm. The average error of all reconstructed sample points is 0.72 cm.

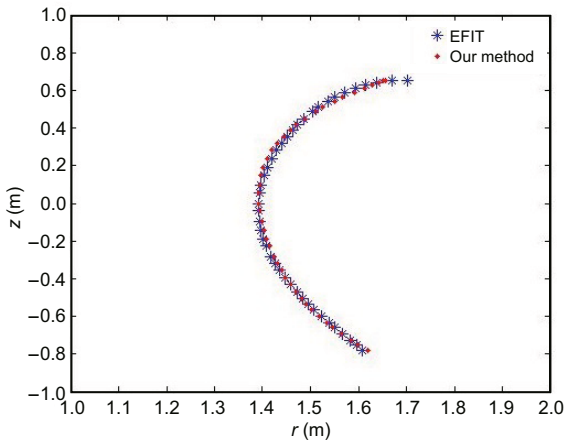

Fig. 9 Optical reconstruction results of the 5.74 s image of a 52 039-shot discharge video

4.2 Global optimization reconstruction of multiple frames

Plasma boundary reconstruction of a single frame has been introduced in Section 4.1. Obviously, the coefficient vector $\boldsymbol{a}$ varies from frame to frame. The image of each frame can be determined by transformation matrix $\boldsymbol{W}$, which is the optimal solution for the corresponding frame and cannot reconstruct the plasma boundary of other frames. However, the ultimate goal is to solve the global optimal solution $\widetilde{\boldsymbol{W}}$ for all frames, and $\widetilde{\boldsymbol{W}}$ can be solved by the iteration method. Suppose the polynomial coefficient vector of the boundary of frame c image is $\boldsymbol{a}_c$, and the transformation matrix obtained is $\boldsymbol{W}_c$. The average error of reconstruction is defined as

$$\text{error}_c = \frac{1}{j}\sum_{k=1}^{j} |\boldsymbol{a}\widetilde{\boldsymbol{W}}\boldsymbol{z}_k - r_k|. \tag{15}$$

After normalization, the iteration formula obtained is

$$\widetilde{\boldsymbol{W}} = \frac{\sum \text{error}_c \widetilde{\boldsymbol{W}}_c}{\sum \text{error}_c}. \tag{16}$$

The iterative initial value can be set as $\boldsymbol{W}_1$ or the average of $\boldsymbol{W}$. Then set the number of iterations or iterative stopping condition to end the iterative cycle, so it can obtain a final global optimal solution $\widetilde{\boldsymbol{W}}$. Experimental results show that this method usually reaches convergence quickly; in this study, we simply iterate 30 times to end the loop.

The sample database should be established, including a training sample and a test sample. The training sample is used to solve $\widetilde{\boldsymbol{W}}$ and the test sample is used to evaluate the effects of reconstruction. In this study, 20 groups of discharge videos and corresponding EFIT results are divided into two equal and random sample databases, but not every frame of the image will be used as a sample. EAST's video capture system uses two high-speed CCD cameras, whose frame rates can reach 100 frames/s, whereas the actual frequency of EFIT is just 12.5 Hz. Thus, some frames can be extracted as samples and they meet the following requirements: (1) In the stable period of plasma discharge, the image has a clear and stable plasma boundary; (2) Time is consistent with EFIT.

Based on the two requirements above, each Tokamak discharge video removes the frame of the rising period and falling period, and it takes a total of 71 data images every 80 ms from 2.46 s to 8.06 s. Some discharge videos have 1 to 2 defective frames of EFIT reconstruction data. Finally, the training sample database contains 704 samples and the test sample database contains 696 samples. Each sample includes the binary image containing the extracted edge, the inner boundary coordinates reconstructed by EFIT, and the time stamp.

The global optimization reconstruction includes horizontal drift of an uncertain value. There is no doubt that there must be an error in reconstruction. If the error is presented mainly in the coefficient terms of coefficient vector $\widetilde{\boldsymbol{b}}$, the reconstructed boundary will have a shape distortion. However, if the error is presented mainly in the constant term, the reconstructed boundary will have a horizontal drift. The experiment results show that the order of magnitude of constant term $\widetilde{b}_1$ is much greater than that of the coefficient term. Thus, $\widetilde{b}_1$ has a large absolute error, but a small percentage error.

The essence of horizontal drift is that the error is presented mainly in $\widetilde{b}_1$. Reducing the error of the constant term is bound to increase the errors of the coefficient terms. After analysis, the position of the left pole ($z = 0$) of the plasma boundary is almost unchanged. Thus, this special point can be used to achieve horizontal drift correction (HDC). When $z = 0$, $r \in (1.3877, 1.4275)$ m in all 1400 sample data. The average of r is 1.4079 m. Assuming that $\widetilde{r}$ is 1.4079 m when $z = 0$, we can calculate the distance of horizontal drift and the final reconstruction result

as follows:

$$\text{offset} = \widetilde{b}_1 - 1.4079, \tag{17}$$

$$\widetilde{r}_k = \boldsymbol{a}\widetilde{\boldsymbol{W}}\boldsymbol{z}_k - \text{offset}. \tag{18}$$

The maximum error of this approach is theoretically 2 cm, which is within an acceptable range. The horizontal drift is not solved constitutionally, but the error has been reduced within an acceptable range for a feedback control system. Table 2 shows the reconstruction results of test sample databases with HDC. Obviously, the reconstruction errors are greatly reduced after HDC. Fig. 10 shows an example of reconstruction results.

Table 2 Errors of global reconstruction with horizontal drift correction (HDC)

Type	Error (m)		
	Maximum	Average	Minimum
Original	1.1551	0.2549	0.0083
HDC	0.0802	0.0249	0.0072

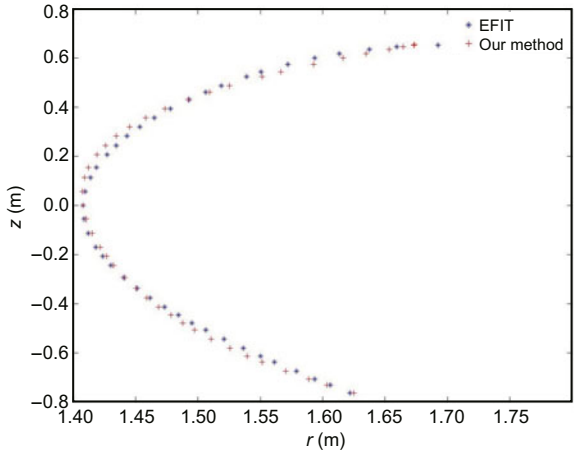

Fig. 10 Global optimization reconstruction results with horizontal drift correction

4.3 Discussion of the reconstruction order

The polynomial order of our proposed model is four. Different orders are applied to the reconstruction model to analyze the influence of the fitting order for reconstruction in the following. Table 3 shows the results.

With an increase of the order of fitting polynomial, the maximum reconstruction error and the average reconstruction error gradually increase, whereas the minimum reconstruction error decreases. With the order increasing, the increasing number of the unknown parameters of matrix $\widetilde{\boldsymbol{W}}$ means that the reconstruction model becomes more sensitive. A high-order polynomial can express the plasma boundary more accurately. When the extracted edge and transition matrix $\widetilde{\boldsymbol{W}}$ are fairly accurate, the algorithm can reconstruct the boundary coordinates well in the poloidal plane. Otherwise, the reconstruction error will be significantly enlarged. Fig. 11 proves this conclusion. The reconstruction error of the 531$^{\text{st}}$ frame is the largest of all samples. In Figs. 11a, 11b, and 11c, the error gradually increases with the increase of the fitting order. When reconstruction error is not very large, such as that in the 399$^{\text{th}}$ frame, the error gradually decreases with the increase of the fitting order.

Table 3 Final reconstruction errors of different orders for global reconstruction

Order	Error (m)		
	Maximum	Average	Minimum
2	0.0285	0.0154	0.0105
3	0.0527	0.0164	0.0073
4	0.0802	0.0249	0.0072

Different order reconstruction models have their own advantages and disadvantages. Low-order reconstruction cannot guarantee that the results of the optical reconstruction almost coincide with the original EFIT data; however, it can ensure that the effects of reconstruction will not be poor even in the case of large errors. In other words, accuracy is not high but robustness is better. On the contrary, high-order reconstruction can ensure that the reconstruction effect is particularly good in most cases; however, once an error occurs, it will be enlarged obviously. High-order reconstruction has a high degree of accuracy but it is less robust. Because low- and high-order reconstructions have their own advantages, laboratory personnel should choose the appropriate order depending on the circumstances.

The total EAST Tokamak plasma boundary optical reconstruction process requires less than 50 ms using an Intel Core i7-4710MQ PC with 8 GB RAM in MATLAB. The EAST Tokamak control computer has significantly higher calculation speed. Using more efficient programming language and multithread programming techniques will vastly reduce

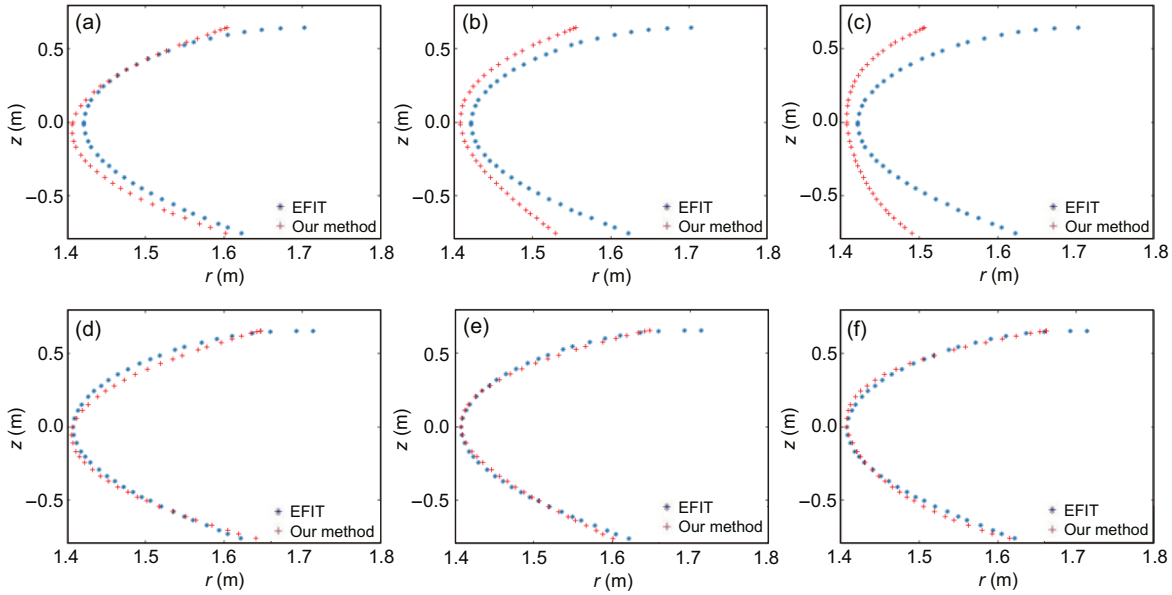

Fig. 11 Comparison of the reconstruction of different fitting orders: 531st frame with the second order (a), the third order (b), and the fourth order (c); 399th frame with the second order (d), the third order (e), and the fourth order (f)

the required time consumption. In C++ compiled version, the time consumption is less than 1 ms, which is much less than a two-frame interval of a CCD camera, so our method can achieve real-time reconstruction.

5 Conclusions and future work

In this paper, we have described the EAST Tokamak optical plasma boundary reconstruction including plasma boundary detection and plasma boundary reconstruction. Because the plasma boundary changes slowly, we propose an edge detection algorithm based on global contrast to extract the plasma boundary. Compared with traditional edge detection algorithms based on a gradient operator and the edge detection algorithm of the TCV Tokamak, our method can more accurately extract a unique and clear plasma boundary. Without camera calibration, we propose a plasma boundary reconstruction model based on the least squares method to transform the extracted boundary from the image plane to the Tokamak poloidal plane. The reconstruction error is about 1–2 cm and the time required is less than 50 ms (using an Intel Core i7-4710MQ PC with 8 GB RAM in MATLAB). The polynomial order has an influence on the reconstruction results. High-order reconstruction has higher accuracy, whereas low-order reconstruction is more robust.

Some unsolved issues are expected to be researched further. The optical system should be improved for higher-quality images. Currently, it is difficult to clearly capture the outer plasma boundary, which makes reconstructing the outer boundary impossible. Further work is needed to extract the full boundary. In addition, horizontal drift should be solved constitutionally for better accuracy.

References

Ahn JW, Maingi R, Mastrovito D, et al., 2010. High speed infrared camera diagnostic for heat flux measurement in NSTX. *Rev Sci Instrum*, 81(2):023501. https://doi.org/10.1063/1.3297899

Alpers A, Gritzmann P, Moseev D, et al., 2015. 3D particle tracking velocimetry using dynamic discrete tomography. *Comput Phys Commun*, 187:130-136. https://doi.org/10.1016/j.cpc.2014.10.022

Canny J, 1986. A computational approach to edge detection. *IEEE Trans Patt Anal Mach Intell*, 8(6):679-698. https://doi.org/10.1109/TPAMI.1986.4767851

Davis WM, Patel RI, Boeglin WU, 2010. Advances in fast 2D camera data handling and analysis on NSTX. *Fus Eng Des*, 85(3):325-327. https://doi.org/10.1016/j.fusengdes.2010.02.005

Hommen G, Baar MD, Nuij P, et al., 2010. Optical boundary reconstruction of tokamak plasmas for feedback control of plasma position and shape. *Rev Sci Instrum*, 81(11):113504.
https://doi.org/10.1063/1.3499219

Hommen G, de Baar M, Citrin J, et al., 2013. A fast, magnetics-free flux surface estimation and q-profile reconstruction algorithm for feedback control of plasma profiles. *Plasma Phys Contr Fus*, 55(2):025007.
http://stacks.iop.org/0741-3335/55/i=2/a=025007

Hommen G, de Baar M, Duval BP, et al., 2014. Real-time optical plasma boundary reconstruction for plasma position control at the TCV Tokamak. *Nucl Fus*, 54(7):073018.
https://doi.org/10.1088/0029-5515/54/7/073018

Hussain S, Qayyum A, Ahmad Z, et al., 2016. Initial plasma formation in the GLAST-II spherical Tokamak. *J Fus Energy*, 35(3):529-537.
https://doi.org/10.1007/s10894-015-0052-z

Kumar D, Clayton DJ, Parman M, et al., 2012. Dual transmission grating based imaging radiometer for Tokamak edge and divertor plasmas. *Rev Sci Instrum*, 83(10):10E511.
https://doi.org/10.1063/1.4732182

Martin V, Travere JM, Bremond F, et al., 2010. Thermal event recognition applied to protection of Tokamak plasma-facing components. *IEEE Trans Instrum Meas*, 59(5):1182-1191.
https://doi.org/10.1109/TIM.2009.2038032

Mitteau R, Spruytte J, Vallet S, et al., 2007. A possible method of carbon deposit mapping on plasma facing components using infrared thermography. *J Nucl Mater*, 363-365:206-210.
https://doi.org/10.1016/j.jnucmat.2007.01.009

Munsat T, Zweben SJ, 2006. Derivation of time-dependent two-dimensional velocity field maps for plasma turbulence studies. *Rev Sci Instrum*, 77(10):103501.
https://doi.org/10.1063/1.2356851

Odstrcil M, Mlynár J, Weinzettl V, et al., 2013. Dust observation in the compass Tokamak using fast camera. 22nd Annual Conf of Doctoral Students, p.73-79.

Perek P, 2013. High-performance image processing system for plasma diagnostics. Int PhD Workshop OWD, p.328-331.

Pironti A, Walker M, 2005. Fusion, Tokamaks, and plasma control: an introduction and tutorial. *IEEE Contr Syst*, 25(5):30-43.
https://doi.org/10.1109/MCS.2005.1512794

Qi P, Li Q, Luo GN, 2008. Application of infrared thermography in NDT of plasma-facing components for Tokamaks. 17th World Conf on Non-destructive Testing, p.1-8.

Xue E, Luo J, Shu S, et al., 2011. Plasma edge detection and tracking in the east superconducting Tokamak discharge. 3rd Int Conf on Measuring Technology and Mechatronics Automation, p.865-868.
https://doi.org/10.1109/ICMTMA.2011.499

Zhang Z, 2000. A flexible new technique for camera calibration. *IEEE Trans Patt Anal Mach Intell*, 22(11):1330-1334.
https://doi.org/10.1109/34.888718

Zhu Y, Xie J, Liu WD, et al., 2016. The general optics structure of millimeter-wave imaging diagnostic on Tokamak. *J Instrum*, 11(1):P01004.
https://doi.org/10.1088/1748-0221/11/01/P01004

Zweben SJ, McChesney J, Gould RW, 2011. Optical imaging of edge turbulence in the Caltech Tokamak. *Nucl Fus*, 23(6):825-830.
https://doi.org/10.1088/0029-5515/23/6/010